Appl Phys B
DOI 10.1007/s00340-009-3449-4

Applied Physics B
Lasers and Optics

Characterization of femtosecond pulses via transverse second-harmonic generation in random nonlinear media

J. Trull · S. Saltiel · V. Roppo · C. Cojocaru · D. Dumay · W. Krolikowski · D.N. Neshev · R. Vilaseca · K. Staliunas · Y.S. Kivshar

Received: 29 December 2008 / Revised version: 17 January 2009

Abstract We study, both experimentally and theoretically, the process of second-harmonic generation by two non-collinear beams in ferroelectric crystals with a disordered distribution of ferroelectric domains. We show that this parametric process results in generation of second-harmonic wave in the direction transverse to the propagation of the fundamental beam. We demonstrate how this effect can be used for the femtosecond pulse characterization enabling the estimation of both width and chirp of the pulse.

PACS 42.65.-k · 42.65.Ky · 42.25.Fx

1 Introduction

The use of ultrashort optical pulses has nowadays become an essential tool in a rapidly increasing number of applications in both research and industry. Important examples include the measurements of the dynamics of complex DNA molecules, monitoring of chemical reactions, optical communications, and laser micromachining. For the success of such applications, it is essential to obtain precise knowledge of the duration and stability of the laser pulses. The existing techniques of ultrashort pulse measurements usually rely on optical gating between the pulse and its replica that is typically realized through a nonlinear optical process, e.g. parametric process of the generation of the second harmonics [1–5].

Among the different schemes for optical gating, non-collinear second-harmonic generation (SHG) is known as one of the best methods for single-shot pulse-duration measurements [6–21]. In this method, two beams cross at a small angle inside a quadratic nonlinear crystal and, if the phase-matching conditions are fulfilled, a second-harmonic (SH) beam is generated in forward direction. The spatial shape of the generated SH beam represents the correlation function of the interacting ultrashort pulses.

It is well known that to obtain an efficient SHG the phase-matching condition has to be fulfilled. This is usually achieved through techniques such as crystal birefringence [22], periodic photonic materials [23], or quasi-phase matching (QPM) [24–26]. Since the angular, frequency, or temperature conversion bandwidth utilized in these techniques is quite narrow (it decreases with the crystal length), this requires careful selection and alignment of the crystals used in a particular application.

Recently, it was shown that quadratic nonlinear processes can be phase matched in media consisting of antiparallel nonlinear ferroelectric domains with random sizes and spatial distribution. In such types of disordered media, SHG phase matching is possible over a broad frequency bandwidth, being limited only by the transparency region of the crystal, and it does not require angular or thermal crystal

J. Trull · V. Roppo · C. Cojocaru · D. Dumay · R. Vilaseca · K. Staliunas
Departament de Fisica i Enginyeria Nuclear, Universitat Politécnica de Catalunya, 08222 Terrassa (Barcelona), Spain

S. Saltiel
Faculty of Physics, Sofia University, 1164 Sofia, Bulgaria

S. Saltiel · W. Krolikowski (✉) · D.N. Neshev · Y.S. Kivshar
Nonlinear Physics Center and Laser Physics Center, Center for Ultrahigh Bandwidth Devices for Optical Systems (CUDOS), Research School of Physics and Engineering, Australian National University, Canberra, ACT 0200, Australia
e-mail: wzk111@rsphysse.anu.edu.au

K. Staliunas
Institució Catalana de Recerca i Estudis Avançats (ICREA), Barcelona, Spain

Published online: 06 March 2009

tuning [27]. Needle-like ferroelectric domains are oriented along the Z-axis (c-axis) of the crystal, creating an effective two-dimensional nonlinear structure with a constant linear refractive index, but with randomly alternating sign of the nonlinear $\chi^{(2)}$ tensor components. Such structures can be considered to be composed of an infinite number of $\chi^{(2)}$ gratings with the corresponding reciprocal vectors having random magnitudes and orientations within the XY-plane.

An example of such disordered nonlinear media is an unpoled strontium barium niobate crystal (SBN) with typical domain sizes ranging between 1 and 8 µm [28, 29]. Depending on the direction of propagation of the fundamental beam, the SHG takes place either in the form of a plane (when propagating perpendicularly to the c-axis) [30–32] or a cone (for any other directions). Furthermore, it has been shown that two-beam interactions can be observed in such crystals [33]. In particular, planar noncollinear SHG where the SH signal is emitted in the plane perpendicular to the plane defined by both beams, has been observed [34].

In this work, we show that the planar SHG resulting from the non-collinear interaction of a pulse with its own replica represents the autocorrelation of the pulse. Since the fundamental pulse broadens with the propagation inside the crystal due to material dispersion, the autocorrelation trace will widen correspondingly. This effect can be used for the chirp characterization of the input femtosecond pulses. The broad conversion bandwidth provided by the random QPM process makes possible to use the same crystal for different wavelengths without need of realignment.

2 Model

We consider two fundamental beams propagating in the crystallographic plane XZ of an SBN crystal with the angles $-\alpha$ and $+\alpha$ to the X-axis. Each one of the fundamental beams generates a SH wave which is emitted in the form of a cone at the particular angle for which the phase-mismatch in the direction of the c-axis is compensated [31]. In addition, the interaction between the two fundamental beams intersecting inside the crystal gives rise to a noncollinear SH emission in the plane perpendicular to the c-axis (Z-axis) as schematically shown in Fig. 1. This planar emission appears as a result of the phase matching of the SHG process at any direction within the XY-plane due to the continuous set of reciprocal lattice vectors provided by the randomness of ferroelectric domain distribution. In particular, the SH emission can be observed not only in forward but also in transverse direction. The SH signal can be detected by a CCD camera imaging the crystal XZ-plane from above (Fig. 1). In this way, the camera records the evolution of the SH signal along the propagation of the fundamental beams from the entrance to the output of the sample.

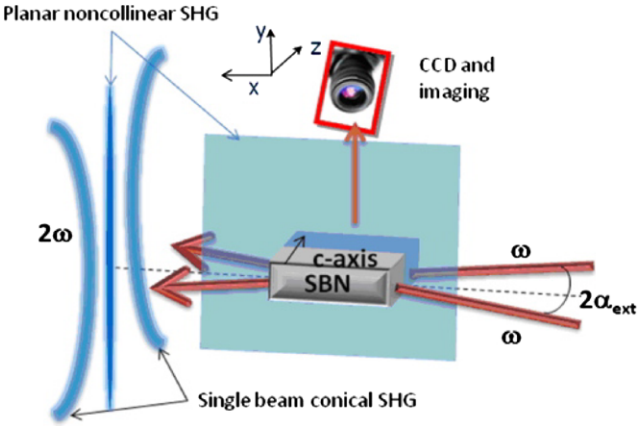

Fig. 1 Schematic presentation of the interacting geometry

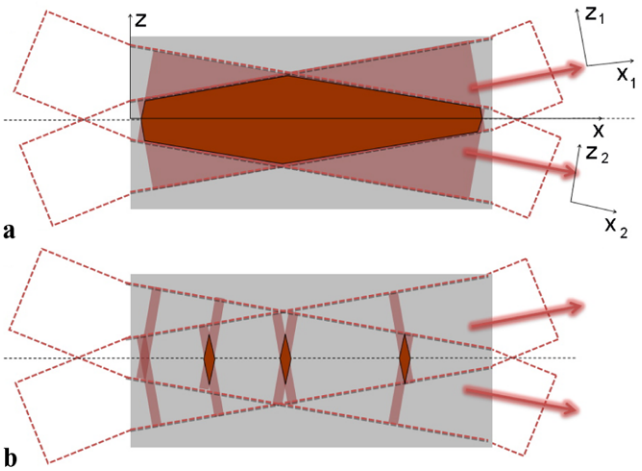

Fig. 2 Beam superposition inside the SBN crystal for the two limiting cases of (**a**) long pulses and (**b**) short pulses. For case (**b**), as beams propagate, the emission region moves along the X-axis, giving rise to the recorded trace

In order to model the generated SH trace we assume that the two fundamental beams have a Gaussian spatial and temporal profile and cross at an angle 2α inside the crystal. The corresponding amplitudes can be written as

$$A_1 = A_{10}\exp\left(-\frac{z_1^2}{2\rho^2}\right)\exp\left(\frac{-(t-x_1/u)^2}{2T^2}\right), \tag{1}$$

$$A_2 = A_{20}\exp\left(-\frac{z_2^2}{2\rho^2}\right)\exp\left(\frac{-(t-x_2/u)^2}{2T^2}\right), \tag{2}$$

where (x_1, z_1) and (x_2, z_2) are the coordinates in reference systems oriented along the propagation direction of each one of the beams (Fig. 2), $u = c/n$ is the speed of light in the crystal. There ρ and T are half beam and pulse width at $1/e$ levels in intensity, respectively.

By introducing a common coordinate system for both beams, corresponding to the X- and Z-axis (x, z) (Fig. 2) we calculate the SH field generated in the crystal. Assum-

ing that phase matching is provided by the random QPM process [35], the SH amplitude is proportional to the nonlinear polarization at doubled frequency:

$$B(x,z,t) \propto P^{(2)}(2\omega) \propto d_{\text{eff}}^{(2)} A_1 A_2. \tag{3}$$

We have already shown [31] that the generated second-harmonic signal recorded by a CCD camera actually represent a cross-correlation function of two interacting pulses. Therefore, in the case of Gaussian pulses, the SH field can be represented as

$$B(x,z,t) = B_0(x) \exp\left(-\frac{z^2\cos^2\alpha + x^2\sin^2\alpha}{\rho^2}\right) \times \exp\left(-\frac{(tu - x\cos\alpha)^2 + z^2\sin^2\alpha}{u^2 T_c^2(x)}\right), \tag{4}$$

where α denotes the half angle between the wave vectors of the two intersecting fundamental beams inside the crystal and $B_0(x)$ is an amplitude that will be described below.

With propagation inside the crystal the pulses experience broadening due to material dispersion, that depends on the initial chirp of the pulse. We have considered this effect assuming a chirped pulse (with initial chirp C at the entrance of the crystal) in a medium with group velocity dispersion β_2 by formally replacing in (4) the pulse duration, T, by the "complex pulse duration", T_c [36], $T_c^2 = [T^2 - i\beta_2 x(1+iC)](1+iC)^{-1}$. In such case $B_0(x) \propto d_{\text{eff}}^{(2)} A_{10} A_{20}/[1 - i\beta_2 x(1+iC)/T^2]$.

For a broad distribution of the domain sizes, the phase-matching condition will be fulfilled for all directions inside the XY-plane. The generated SH signal is emitted from the overlapping region of the fundamental beams inside the crystal in form of a plane as can be seen in Figs. 1 and 2. This overlapping region is then determined by the spatial extent of the beam and by the temporal duration of the pulses. For long pulses, when $T \gg 2\rho\tan\alpha/u$, the overlapping region is limited by the spatial dimensions of the beams (corresponding to the big rhombus shown in Fig. 2(a)). In the case of short pulses, $T \ll 2\rho\tan\alpha/u$, the overlapping region is limited by the pulse lengths only and has a form of a small dark rhombus shown in Fig. 2(b).

Figure 3(a) illustrates emission of the SH (central peak (in blue)) via the noncollinear interaction of the overlapping pulse fronts of the two fundamental beams inside the crystal as described by (4) under the condition of "big" radii ($\rho \gg uT/2\tan\alpha$) of the beams. The graph also shows the background emission of the SH (in pink) by each individual beam. Only in the region of pulse overlap, a much stronger SH signal is emitted. Since the detected signal corresponds to an integration in the time domain, it results in a recorded continuous trace along the X-direction. The resulting SH intensity emitted due to the overlap of the fundamental beams

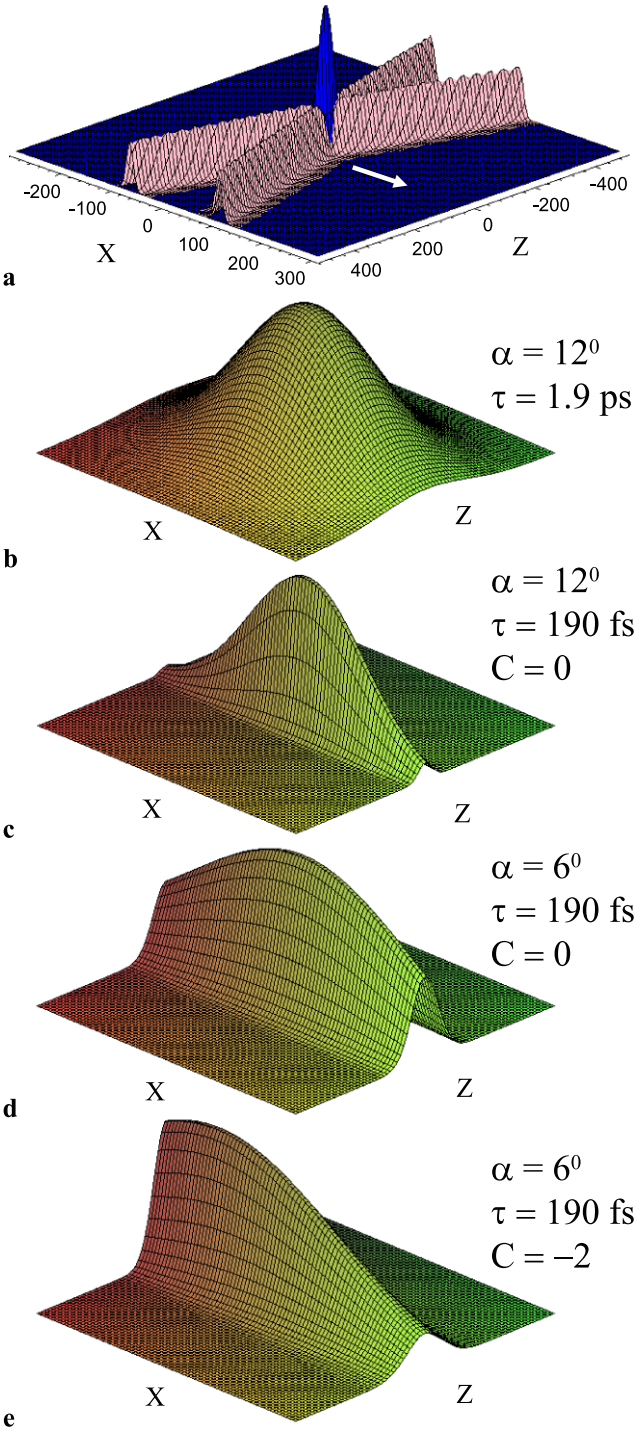

Fig. 3 (**a**) Emission of the SH wave (central peak, *blue*) via the noncollinear interaction of the overlapping fundamental pulses inside the crystal, as described by (4). Background emission of the SH wave by each beam is shown as well. In this simulation, the beam radii are considered much bigger than $uT/2\tan\alpha$, with 2α being the angle between the beams inside the crystal. (**b**–**e**) Theoretically evaluated snap shot of the spatial profiles of the SH signal for different pulse durations and chirp parameters

is given by

$$I_{2\omega}(x,z) = \frac{T^4 I_{2\omega}(0)}{T_{\rm ch}^4(x+L/2)} \exp\left(-\frac{2z^2\sin^2\alpha}{u^2 T_{ch}^2(x+L/2)}\right) \times \exp\left(-\frac{2z^2\cos^2\alpha + 2x^2\sin^2\alpha}{\rho^2}\right), \quad (5)$$

where

$$T_{\rm ch}(x) = T\left[\left(1+\frac{C\beta_2 x}{T^2}\right)^2 + \left(\frac{\beta_2 x}{T^2}\right)^2\right]^{1/2}. \quad (6)$$

If the pulse is "long" the recorded trace corresponds to the second exponent of (5) and its shape (see Fig. 3(b)) is defined only by the transverse dimensions of the beam and can not be used for estimation of pulse duration. In the most interesting, from the practical application point of view limit, of very large ρ, the transverse profile of the SH trace along X is determined solely by the first exponent in (5). This case is illustrated on Fig. 3(c, d, e) for two different angles between the two fundamental beams. If a variable time delay is introduced for one of the pulses the SH line appears moving along the Z-direction. The thickness $\Delta z(x)$ of the SH trace depends directly on the pulse duration

$$\Delta z(x) = \frac{u T_{\rm ch}(x)}{\sqrt{2}\sin\alpha}. \quad (7)$$

If the width of the SH trace is measured at the input facet of the crystal ($x = 0$) we obtain (considering $T_{\rm ch}(0) = T$) a measure of the pulse duration,

$$T = \left(\sqrt{2}\sin\alpha\right)\Delta z(0)/u. \quad (8)$$

The same relation holds for the experimentally measurable FWHM of the pulse duration, τ, and the FWHM of the trace transverse profile, $\tau = (\sqrt{2}\sin\alpha_{\rm ext})\Delta z_{\rm FWHM}(0)/c$.

Additional information about the pulse can be obtained if the SH trace is recorded along the nonlinear crystal. Depending on the values of the group velocity dispersion β_2 and the initial chirp of the pulse C, the width of the trace may became dependent on the distance measured from the entrance surface. For β_2 and C having the same sign, the trace width will grow constantly with the increase of distance from the front surface, while for β_2 and C of the opposite signs, this width will first reach its minimum at certain distance and will start growing afterwards. The case of negative $\beta_2 = -466$ fs^2/mm and $C = -4$ is shown on Fig. 3(e). As can be seen from (6) and (7) for known β_2 it is sufficient to measure the width of the trace at a distance x from the crystal entrance in order to determine the initial chirp of the pulse:

$$C = \frac{\sqrt{(4\Delta z(0)^2\Delta z(x)^2/u^4)\sin^4\alpha - (x\beta_2)^2}}{x\beta_2} - \frac{(2\Delta z(0)^2/u^2)\sin^2\alpha}{x\beta_2}. \quad (9)$$

Comparing Figs. 3(d) and 3(e) we note that the chirp may strongly affect the spatial profile of the recorded second-harmonic field, which can be also used in analyzing the properties of the input pulses.

3 Experimental results and discussions

We have used the method described above to estimate the width and initial linear pulse chirp of femtosecond pulses generated by a Ti:Sapphire fs oscillator (Mira, Coherent) operating at 810 nm, with a pulse duration of 180 fs, and a repetition rate of 76 MHz. The incident extraordinary polarized beam is split in two parts (see Fig. 4) which are incident on an as-grown unpoled SBN:61 crystal ($5 \times 5 \times 10$ mm, all sides polished, purchased from Altechna Co. Ltd.) under a given angle. The half-wave plate P was used to adjust the intensity splitting ratio in the two arms. The crossing angle, $2\alpha_{\rm ext}$, and the beam widths are selected in order to satisfy the relation $\rho \gg uT/2\tan\alpha$. In different experiments this angle ranged from 10 to 28 degrees. A variable delay line in one of the arms ensures that the two pulses coincide inside the crystal. In addition, this delay line can be used to calibrate the temporal scale of the measurements. Changing the pulse delay by a known amount δt, induces displacement of the correlation trace in the Z-direction $\delta z = u\delta t/(2\sin\alpha)$, which can be precisely measured.

We note that the bisector of the angle between two fundamental beams has to be aligned to coincide (within 1°–2°) with the crystal X-axis. While this alignment is not critical, it ensures that the SH radiation resulting from the mixing of the two beams will form a plane coinciding with XY crystal plane.

It should be stressed that since the SH signals originating from each individual beam are emitted in a cone, it is possible to separate them from the emission coming from

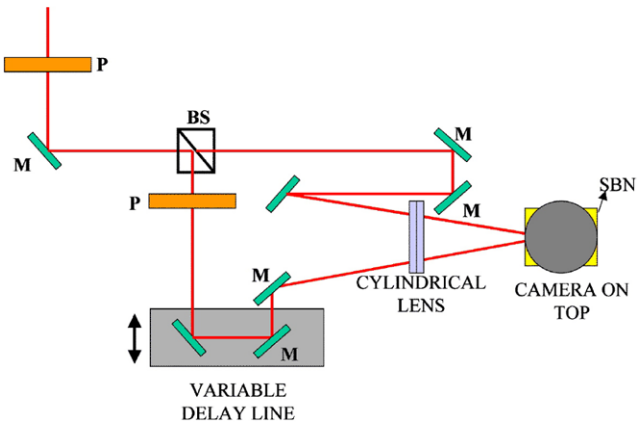

Fig. 4 Experimental setup. M—mirror, BS—polarizing beam splitter, P—half-wave plates

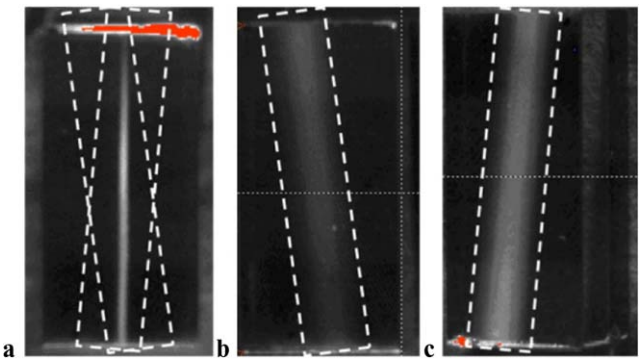

Fig. 5 Recorded SH traces corresponding to (**a**) noncollinear planar SHG and (**b**, **c**) single beam SHG. To obtain the images (**b**) and (**c**), the imaging system is rotated in the YZ-plane

the overlapping pulses which is generated in a plane. This makes the measurement virtually background-free, as illustrated in Fig. 5. Figure 5(a) shows the background-free autocorrelation trace recorded by the camera pointing vertically at the crystal. The images in Figs. 5(b, c) depict SH signals emitted by each separate beam. These images were obtained by *tilting* the camera at an angle corresponding to the conical emission of the SH by each fundamental beam.

Figures 6(a, b) depict the image of the autocorrelation trace together with its transverse profile dependence as a function of the distance from the entrance facet of the crystal. In this particular case, (7) yields the pulse width $\tau = 193$ fs at the entrance facet of the crystal, and 40% more, 270 fs, at the output facet of the crystal. The photo in Fig. 6(c) illustrates the experimental observation of the SH cross-correlation trace originating from interaction of a single pulse in a one beam with two consecutive pulses in the other beam. In this case the interaction results in a formation of two parallel SH traces separated by a distance corresponding to the temporal separation of both pulses. The temporal delay between the pulses is 837 fs. Graph in Fig. 6(d) depicts schematic of this process. We mention that the accuracy of this measurement depends on the resolution of the imaging system which can be easily controlled by choosing the proper magnification. In our experiments all autocorrelation traces were recorded using a standard CCD camera (such as, e.g. AVT Marlin, IEEE 1394, resolution 656(h) × 494(v), by Allied Vision Technologies). To asses the accuracy of our method we compared its results with those obtained by the commercial Grenouille FROG. We found very good correspondence in pulse measurements. For instance, for a Grenouille reconstructed autocorrelation FWHM of 272.2 fs, our method gave 276 fs.

As was mentioned above, the noncollinear SHG geometry discussed here enables us not only to determine the pulse width but also to obtain information about the initial pulse chirp. To this end, we should measure the transverse width

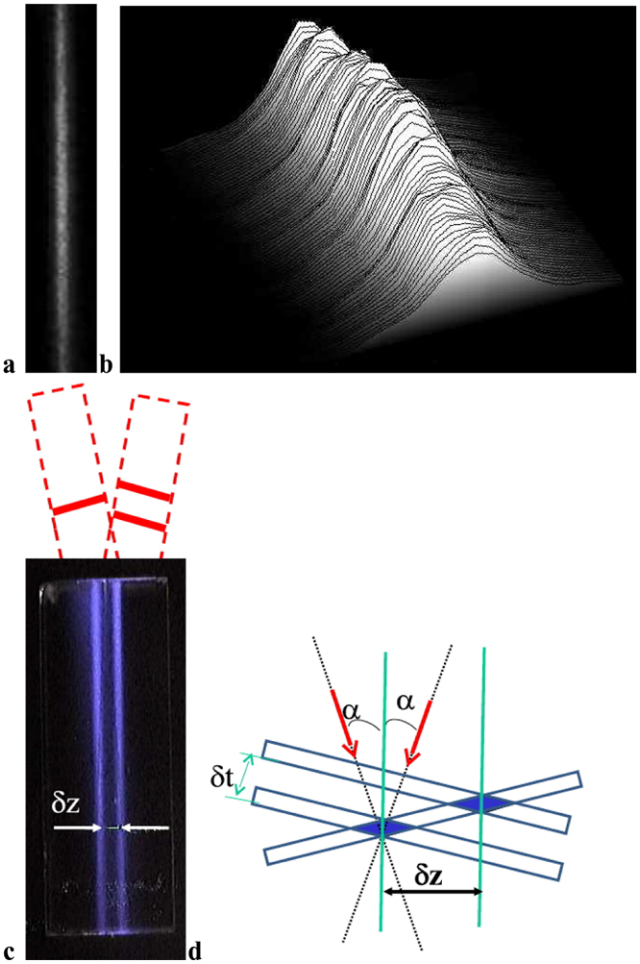

Fig. 6 (**a**) Recorded SH trace for two incident fundamental beams at 810 nm and (**b**) its corresponding transverse profile. (**c**) Experimental observation of the formation of cross-correlation trace, when one of the fundamental beams carries a sequence of two consecutive pulses. (**d**) Schematic illustration of this process

of the autocorrelation trace at different distances from the front entrance facet of the crystal and then use (7) and (9) to calculate the chirp parameter C. We demonstrate this in our experiments using pulses with different initial chirps, realized through different alignment of the laser. The results are shown in Fig. 7, which depicts the width of the autocorrelation signal (data points) as a function of propagation distance. The lines represent a theoretical fit (using (7)) from which the chirp parameter C is found. The insets show corresponding autocorrelation traces.

An additional advantage of using random QPM with respect to other usual nonlinear techniques is that we can obtain a SH signal for different polarizations of the input beam without any further alignment. As expressed in (3), the resulting SH signal is proportional to $d_{\text{eff}}^{(2)}$. The symmetry of the SBN crystal allows for three different interactions, namely (eee), (ooe), and (eoo) [37]. The large bandwidth of the random QPM process allows to simultaneously phase

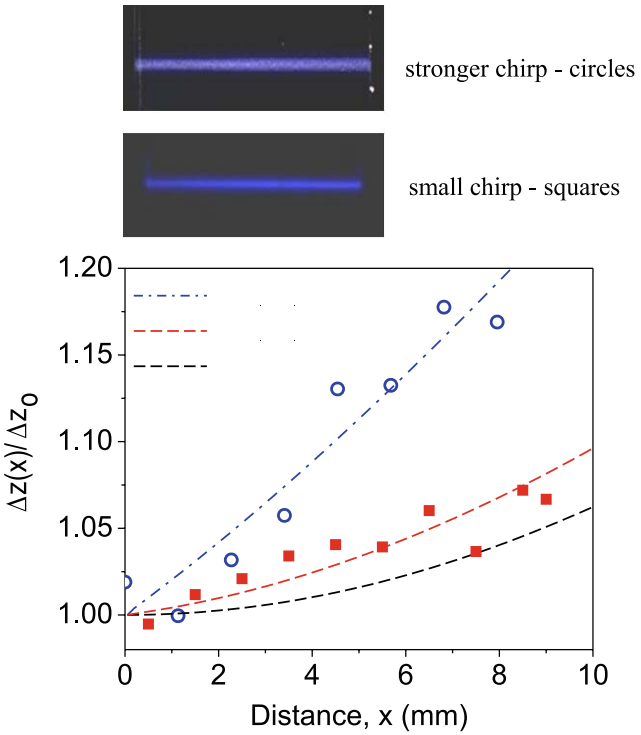

Fig. 7 *Bottom*—evaluation of pulse chirp by measuring the transverse width of the SH trace at different locations inside the crystal. *Dashed lines* represent theoretically calculated evolution of the SH signal for three different values of the incident chirp. *Top*—two typical autocorrelation traces recorded in the regime of weak and strong chirp

match all these processes, so we can obtain a SH planar emission for different input beam polarizations. The most effective SH emission, however, takes place for the extraordinary beams since the (eee) interaction is driven by the largest coefficient d_{33}.

4 Conclusions

We have demonstrated that, by employing random quasi-phase matching [35] in an SBN crystal, we can realize non-collinear planar second-harmonic generation. By imaging the second harmonics emitted in the transverse direction, we have determined the pulse duration and the initial linear pulse chirp. In addition, such type of nonlinear media can be used for nonlinear optical interactions with multiple input wavelengths or input polarizations without any further alignment or angular tuning due to available broad bandwidth provided by the random nonlinear photonic structure.

Acknowledgements This project was partially supported by the Australian Research Council and COST Action MP0702. The authors at Universitat Politecnica de Catalunya thank Ministerio de Educacion y Ciencia for a financial support through Project FIS2005-07931-C03-03 and to the Generalitat de Catalunya for the support through the project 2005SGR00457. Solomon Saltiel thanks the Australian National University and Universitat Politécnica de Catalunya for hospitality.

References

1. J.C. Diels, W. Rudolph, *Ultrashort Laser Pulse Phenomena* (Academic Press, San Diego, 1989)
2. R. Trebino, K.W. DeLong, D.N. Fittinghoff, J.N. Sweetser, M.A. Krumbgel, B.A. Richman, Rev. Sci. Instrum. **68**, 3277 (1997)
3. C. Iaconis, I.A. Walmsley, Opt. Lett. **23**, 792 (1998)
4. C. Dorrer, E.M. Kosik, I.A. Walmsley, Opt. Lett. **27**, 548 (2002)
5. Y.R. Shen, *The Principles of Nonlinear Optics* (Wiley, New York, 1984)
6. R.N. Gyuzalian, S.B. Sogomonian, Z.Gy. Horvath, Opt. Commun. **29**, 239 (1979)
7. C. Kolmeder, W. Zinth, W. Kaiser, Opt. Commun. **30**, 453 (1979)
8. S.M. Saltiel, S.D. Savov, I.V. Tomov, L.S. Telegin, Opt. Commun. **38**, 443 (1981)
9. S.M. Saltiel, S.D. Savov, I.V. Tomov, Opt. Quantum Electron. **14**, 391 (1982)
10. J. Janzsky, G. Corradi, R.N. Gyuzalian, Opt. Commun. **23**, 293 (1977)
11. C. Rempel, W. Rudolph, Exp. Tech. Phys. (Berlin) **37**, 381 (1988)
12. F. Salin, P. Georges, G. Roger, A. Burn, Appl. Opt. **26**, 4528 (1987)
13. R. Wyatt, E. Marinero, Appl. Phys. **25**, 297 (1981)
14. S. Akturk, M. Kimmel, P. O'Shea, R. Trebino, Opt. Express **11**, 491 (2003)
15. G. Szabo, Zs. Bor, A. Mfiller, Appl. Phys. B **31**, 14 (1983)
16. Y. Ishida, T. Yajima, A. Watanabe, Opt. Commun. **56**, 57 (1985)
17. S. Saltiel, K. Stankov, P. Yankov, V. Telegin, Appl. Phys. B **40**, 25 (1986)
18. M. Raghuramaiah, A.K. Sharma, P.A. Naik, P.D. Gupta, R.A. Ganeev, Sadhana **26**, 603 (2001), Part 6
19. J. Collier, C. Danson, C. Johnson, C. Mistry, Rev. Sci. Instrum. **70**, 1599 (1999)
20. A. Dubietis, R. Danielius, A. Stabinis, G. Valiulis, A. Varanavicius, Opt. Commun. **105**, 67 (1994)
21. Z. Sacks, G. Mourou, R. Danielius, Opt. Lett. **26**, 462 (2001)
22. V.G. Dmitriev, G.G. Gurzadyan, D.N. Nikogosyan, *Handbook of Nonlinear Optical Crystals* (Springer, Berlin, 1991)
23. A. Yariv, P. Yeh, J. Opt. Soc. Am. **67**, 438 (1977)
24. J.A. Armstrong et al., Phys. Rev. **127**, 1918–1939 (1962)
25. M.M. Fejer, G.A. Magel, D.H. Jundt, R.L. Byer, IEEE J. Quantum Electron. **28**, 2631 (1992)
26. J.-M. Liu, *Photonic Devices* (Cambridge University Press, Cambridge, 2005), Chap. 9
27. M. Horowitz, A. Bekker, B. Fischer, Appl. Phys. Lett. **62**, 2619 (1993)
28. J.J. Romero, C. Arago, J.A. Gonzalo, D. Jaque, J. Garcia Sole, J. Appl. Phys. **93**, 3111 (2003)
29. M.O. Ramirez, D. Jaque, L. Ivleva, L.E. Bausa, J. Appl. Phys. **95**, 6185 (2004)
30. A.R. Tunyagi, M. Ulex, K. Betzler, Phys. Rev. Lett. **90**, 243901 (2003)
31. R. Fischer, D.N. Neshev, S.M. Saltiel, W. Krolikowski, Y.S. Kivshar, Appl. Phys. Lett. **8989**, 191105 (2006)
32. P. Molina, M.O. Ramirez, L.E. Bausa, Adv. Funct. Mat. **18**, 709 (2008)
33. R. Fischer, D.N. Neshev, S.M. Saltiel, A.A. Sukhorukov, W. Krolikowski, Y.S. Kivshar, Appl. Phys. Lett. **91**, 031104 (2007)

34. V. Roppo, D. Dumay, J. Trull, C. Cojocaru, S. Saltiel, K. Staliunas, R. Vilaseca, D.N. Neshev, W. Krolikowski, Y.S. Kivshar, Opt. Express **16**, 14192 (2008)
35. M. Baudrier-Raybaut, R. Haidar, Ph. Kupecek, Ph. Lemasson, E. Rosencher, Nature (London) **432**, 374 (2004)
36. G.P. Agrawal, *Nonlinear Fiber Optics* (Academic Press, San Diego, 2007), Chap. 3
37. J. Trull, C. Cojocaru, R. Fischer, S. Saltiel, K. Staliunas, R. Herrero, R. Vilaseca, D.N. Neshev, W. Krolikowski, Yu.S. Kivshar, Opt. Express **15**, 15868 (2007)